CSIRO PUBLISHING
www.publish.csiro.au/journals/eg
Exploration Geophysics, 2007, **38**, 60–68

A new algorithm for SIP parameter estimation from multi-frequency IP data: preliminary results

Jeong-Sul Son[1,2] Jung-Ho Kim[1] Myeong-Jong Yi[1]

[1]Engineering Geophysics Group, Korea Institute of Geoscience and Mineral Resources, Daejeon 305-350, Korea.
[2]Corresponding author. Email: jsson@kigam.re.kr

Abstract. Conventional analysis of spectral induced polarization (SIP) data consists of measuring impedances over a range of frequencies, followed by spectral analysis to estimate spectral parameters. For the quantitative and accurate estimation of subsurface SIP parameter distribution, however, a sophisticated and stable inversion technique is required. In this study, we have developed a two-step inversion approach to obtain the two-dimensional distribution of SIP parameters. In the first inversion step, all the SIP data measured over a range of frequencies are simultaneously inverted, adopting cross regularisation of model complex resistivities at each frequency. The cross regularisation makes it possible to enhance the noise characteristics of the inversion by imposing a strong assumption, that complex resistivities should show similar characteristics over a range of frequencies. In numerical experiments, we could verify that our inversion approach successfully reduced inversion artefacts. As a second step, we have also developed an inversion algorithm to obtain SIP parameters based on the Cole–Cole model, in which frequency-dependent complex resistivities from the first step are inverted to obtain a two-dimensional distribution of SIP parameters. In numerical tests, the SIP parameter images showed a fairly good match with the exact model, which suggests that SIP imaging can provide a very useful subsurface image to complement resistivity.

Key words: Cole–Cole model, complex resistivity, cross regularisation, inversion, SIP, SIP parameter.

Introduction

The Induced Polarization (IP) method is a geophysical method that has been primarily used for mineral exploration (Pelton et al., 1978; Fink et al., 1990). Recently, the IP method has been revisited as a promising tool in environmental and engineering applications owing to advances in the instrumentation and modelling or inversion capabilities (Kemna et al., 2000), and some case histories of successful environmental applications can be found in the literature (Weller and Börner, 1996; Vanhala et al., 1992; Börner et al., 1993). Much attention has been given to the spectral IP (SIP) or complex resistivity method, where impedance data are collected over many frequencies, typically in the mHz–kHz range.

Electrical conduction (charge transport) and polarization (charge separation) are fundamental physical properties of subsurface material. A rock or soil can be considered as a three-component system, consisting of grains, pores (which might be fluid-filled), and the corresponding interfaces. The electrical bulk properties of the system depend on both the individual properties of these constituents and their geometrical arrangement. Complex resistivity can describe physical parameters of both conduction and polarization phenomena at frequencies less than 10 kHz. As a frequency-dependent complex number with both magnitude and phase, complex resistivity fully describes the electrical response of a rock or soil to electrical excitation.

Applications of the complex resistivity method are mainly confined to mineral exploration. Recently, there has been growing interest in deriving information about the hydraulic properties of subsurface environments. Olhoeft (1985) performed a frequency-domain analysis to obtain IP parameters from multi-frequency data, and Yuval and Oldenburg (1997) developed a process to estimate Cole–Cole parameters from time-domain IP data. A regularised SIP inversion method for multi-frequency IP data, based on the Cole–Cole model, has also been developed (Routh et al., 1998; Loke et al., 2006). Yang and Kim (2004) introduced a technique for Cole–Cole parameter estimation from inverted complex resistivities. SIP parameters, as well as complex resistivity, are also used to discriminate subsurface characteristics.

These authors introduced various methods to obtain the distribution of SIP parameters from multi-frequency IP data. These methods can be categorised into two types. In the first approach, SIP parameters are directly obtained by the inversion of SIP data, while inverted complex resistivities of the subsurface are used to calculate the spectral parameters in the second approach. The first approach, the direct method, has an advantage in that we can apply many sophisticated constraints or regularisations to obtain geologically meaningful SIP parameters although it is not easy to change the dispersion model. On the other hand, the second approach, the indirect method, provides more flexibility in the choice of dispersion model than first approach, because SIP parameter estimation relies on the choice of an appropriate dispersion model such as the Cole–Cole model. This indirect method, however, can produce more inversion noise or artefacts because regularisation or constraints are not directly applied to the SIP parameter distribution.

In this study, we choose the indirect approach, to have a flexible method for estimation of the SIP parameters. To overcome the noise sensitivity and constraints problems, we develop a new multi-frequency inversion algorithm adopting cross regularisation, which imposes a strong constraint that the inverted complex resistivity distribution should have a

10.1071/EG07009 0812-3985/07/010060

very similar structure over the measurement frequencies. After that we introduce an SIP estimation technique by which SIP parameters are calculated from the inverted complex resistivity results. The inversion and estimation procedure is presented and demonstrated with a synthetic example.

Inversion of multi-frequency IP data

In this study, we developed an inversion algorithm for multi-frequency IP data. Since the inversion of multi-frequency IP data is basically a development of the conventional method using single-frequency data, we describe the basic theory and procedures used in the modelling and inversion of single frequency data first. This basic inversion algorithm is well documented by Kemna et al. (2004) and only a brief description is provided in this paper to facilitate the explanation of multi-frequency inversion algorithm. For forward modelling, a 2.5-dimensional DC resistivity modelling algorithm was modified to cover the general case of complex resistivity.

If the region of interest is assumed to have a two-dimensional complex conductivity distribution $\sigma^*(x, y, \omega)$ (* denotes a complex variable), and electromagnetic induction effects are negligible at the low measurement frequency (typically <10 or 100 Hz, depending on measurement environment), the governing equation is Poisson's Equation which after Fourier transformation becomes

$$\frac{\partial}{\partial x}\left(\sigma^*(\omega)\frac{\partial \phi^*}{\partial x}\right) + \frac{\partial}{\partial z}\left(\sigma^*(\omega)\frac{\partial \phi^*}{\partial z}\right) - k_y^2\sigma^*(\omega)\phi^* = -I\delta(x)\delta(z) \quad (1)$$

where k_y is the Fourier transformation variable corresponding to the assumed strike direction y, $\phi^*(\omega)$ is complex potential in the Fourier domain at the given frequency ω and I is the injected current. In this study, equation (1) is solved numerically by the Finite Element Method (FEM) and after applying appropriate boundary conditions, we arrive at the following system equation to solve for the unknown complex potential:

$$\mathbf{Ax} = \mathbf{b} \quad (2)$$

where $\mathbf{A}$ is a global FEM stiffness matrix, and is a complex symmetric and banded matrix, $\mathbf{x}$ is a complex potential vector to be calculated, and $\mathbf{b}$ is a source vector. This system equation is solved by a numerical library algorithm for complex symmetric matrices.

The solution from equation (2) is inverse Fourier transformed to get complex potential, and geometric factors for a given electrode configuration are multiplied to obtain complex impedance. In this study, we use nine spatial frequencies, sampled linearly in the logarithmic space from 0.0025 to 0.64. Note here that the modelling procedure described above is exactly the same as ordinary DC forward modelling, except that the conductivity and calculated potential are complex variables, and complex algebra was implemented in the DC resistivity modelling code to get the IP response. In inverse modelling, we use the least-squares method with smoothness constraints.

For single-frequency IP inversion, model vector $\mathbf{m}^*$ and the data vector $\mathbf{d}^*$ are defined as

$$m_j^* = \ln \sigma_j^*(\omega) \quad (j = 1, K, M) \quad (4a)$$

$$d_i^K = \ln Z_{i,\mathrm{obs}}^*(\omega) \quad (i = 1, K, N) \quad (4b)$$

where M is the number of parameters, N is the number of IP measurements, and $Z_{i,\mathrm{obs}}^*(\omega)$ denotes the observed impedance at the given frequency. To overcome the inherent non-uniqueness of the inverse problem, a standard smoothness-constrained method (deGroot-Hedlin and Constable, 1990) is used. The objective function to be minimised is composed of the complex L_2-norm of data misfit and model roughness, with the terms being balanced by means of a Lagrange multiplier λ:

$$\Phi(\mathbf{m}^*) = \|\mathbf{d}^* - \mathbf{f}^*(\mathbf{m}^*)\|^2 + \lambda\|\mathbf{W}_m\Delta\mathbf{m}^*\|^2 \quad (5)$$

where $\mathbf{f}^*$ is the operator for forward modelling and $\mathbf{W}_m$ is a matrix evaluating the first-order roughness of $\Delta\mathbf{m}^*$. We use Active Constraint Balancing (ACB) (Yi et al., 2003) to enhance the resolving power of the inversion. In the ACB method, the distribution of Lagrangian multipliers is calculated based on resolution analysis, using parameter resolution and spread functions. The amplitude or absolute value of the spread function is used to evaluate the resolving power in this study, because all the quantities in equation (5) are complex variables except the Lagrangian multiplier. Note here that data weighting is not used, but ACB is implemented instead in this study, which is the only difference from Kemna's approach (2004).

Minimisation of the objective function results in the following complex normal equations.

$$(\mathbf{J}^{*\mathrm{H}}\mathbf{J}^* + \lambda\mathbf{W}_m^{\mathrm{T}}\mathbf{W}_m^{\mathrm{T}})\Delta\mathbf{m}^* = \mathbf{J}^{*\mathrm{H}}[\mathbf{d}^* - \mathbf{f}^*(\mathbf{m})^*] \quad (6)$$

Equation (6) is solved for the model update vector, $\Delta\mathbf{m}^*(\omega)$. Herein, superscripts H and T denote Hermitian and transpose matrices respectively, and $\mathbf{J}^*$ is the complex Jacobian matrix evaluated for the current model $\mathbf{m}^*$ according to

$$J_{ij}^*(\omega) = \frac{\partial f_i^*(\omega)}{\partial m_j^*(\omega)} = \frac{\sigma_j^*(\omega)}{Z_i^*(\omega)}\frac{\partial Z_i^*(\omega)}{\partial \sigma_j^*(\omega)} \quad (7)$$

In this study, the complex Jacobian matrix is calculated using the adjoint equation approach.

For the inversion of multi-frequency data, we need an advanced inversion technique because each single-frequency observation set making up the multi-frequency dataset is decoupled from each other. Although the single-frequency datasets can be related to each other through a theoretical dispersion model, such as the Cole–Cole model, each single-frequency dataset is an independent dataset in itself. Routh et al. (1998) and Loke et al. (2006) introduced inversion algorithms in which Cole–Cole parameters are directly parameterised in the inversion. The disadvantage of the direct approach is that it requires that the dispersion model be given a priori. When the Cole–Cole model is not adequate for the description of spectral IP response, the entire inversion procedure must be repeated from scratch assuming a different dispersion model. Their approaches do not provide this kind of flexibility in the choice of dispersion model.

Since we choose the indirect method for the estimation of spectral parameter, we can use a more flexible method to estimate spectral parameters. A new strategy, however, is needed to invert all the multi-frequency IP data at once, because we should obtain a complex resistivity distribution in the subsurface for each frequency at the same time. Usually in the spectral IP survey, we use several frequencies to compile multi-frequency data. Each IP observation at a single frequency in the multi-frequency dataset is independent of each other in terms of the inversion if some further assumption is not provided. The most important strategy we assume in this study is that the subsurface complex resistivity distribution for each frequency will not show significant differences. To incorporate this strategy into the inversion algorithm, we propose to use cross regularisation,

which maximises the structural similarity of the inverted sections for each frequency. The objective function for multi-frequency inversion can be written as

$$\Phi(\mathbf{m}^*) = \sum_{i=1}^{N_f} \|\mathbf{d}_i^* - \mathbf{f}_i^*(\mathbf{m}_i^*)\|^2 + \sum_{i=1}^{N_f} \lambda_i \left(\|\mathbf{W}_m \Delta\mathbf{m}_i^*\|^2 + \beta \sum_{j=i-1}^{i+1} \|\Delta\mathbf{m}_i^* - \Delta\mathbf{m}_j^*\|^2 \right) \quad (8)$$

where N_f is the number of frequencies used in inversion. In this equation, the first term is the sum of misfits of IP data for individual frequencies, while the second one is the sum of regularisation used in this inversion. The second term consists of two parts, the first of which is the smoothness constraint, while the final term is another constraint added to minimise the difference between the model update vectors for the adjacent frequencies. If the single-frequency data in the multi-frequency dataset is sorted by frequency, the data and corresponding inverted results will show maximum similarity with the adjacent values. By using this regularisation in the inversion, we can effectively suppress random noise in the data because the regularisation emphasises the common structure and reduces erroneous artefacts in the inverted sections. Our strategy seems to be very reasonable because inverted results from each frequency dataset may not be very different from each other in the real world.

Minimising the new multi-frequency objective function in equation (8) results in a set of normal equations having the general form

$$\begin{vmatrix} \mathbf{J}_1^{*\mathrm{H}}\mathbf{J}_1^* + \lambda_1 \begin{pmatrix} \mathbf{W}_m^{\mathrm{T}}\mathbf{W}_m \\ +\beta\mathbf{I} \end{pmatrix} & -\lambda_1\beta\mathbf{I} & \cdots & \mathbf{0} \\ -\lambda_2\beta\mathbf{I} & \mathbf{J}_2^{*\mathrm{H}}\mathbf{J}_2^* + \lambda_2 \begin{pmatrix} \mathbf{W}_m^{\mathrm{T}}\mathbf{W}_m \\ +2\beta\mathbf{I} \end{pmatrix} & \cdots & \mathbf{0} \\ \vdots & \vdots & \ddots & \vdots \\ \mathbf{0} & \mathbf{0} & \cdots & \mathbf{J}_{N_f}^{*\mathrm{H}}\mathbf{J}_{N_f}^* + \lambda_{N_f} \begin{pmatrix} \mathbf{W}_m^{\mathrm{T}}\mathbf{W}_m \\ +\beta\mathbf{I} \end{pmatrix} \end{vmatrix} \times \begin{vmatrix} \Delta\mathbf{m}_1^* \\ \Delta\mathbf{m}_2^* \\ \vdots \\ \Delta\mathbf{m}_{N_f}^* \end{vmatrix} = \begin{vmatrix} \mathbf{J}_1^{*\mathrm{H}}\mathbf{e}_1^* \\ \mathbf{J}_2^{*\mathrm{H}}\mathbf{e}_2^* \\ \vdots \\ \mathbf{J}_{N_f}^{*\mathrm{H}}\mathbf{e}_{N_f}^* \end{vmatrix} \quad (9)$$

The diagonal terms of equation (9) are identical to the individual normal equations for each single-frequency inversion. By setting β to zero, the above equation becomes the compact

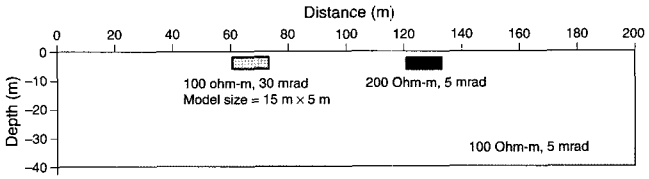

Fig. 1. Simple subsurface model to test the multi-frequency inversion algorithm. The model has two isolated bodies with different characteristics, polarizable and resistive. A total of five sets of IP data are calculated with different noise levels, 30, 10, 5, 2, and 2% respectively. A dipole–dipole array is used with dipole spacing of 5 m.

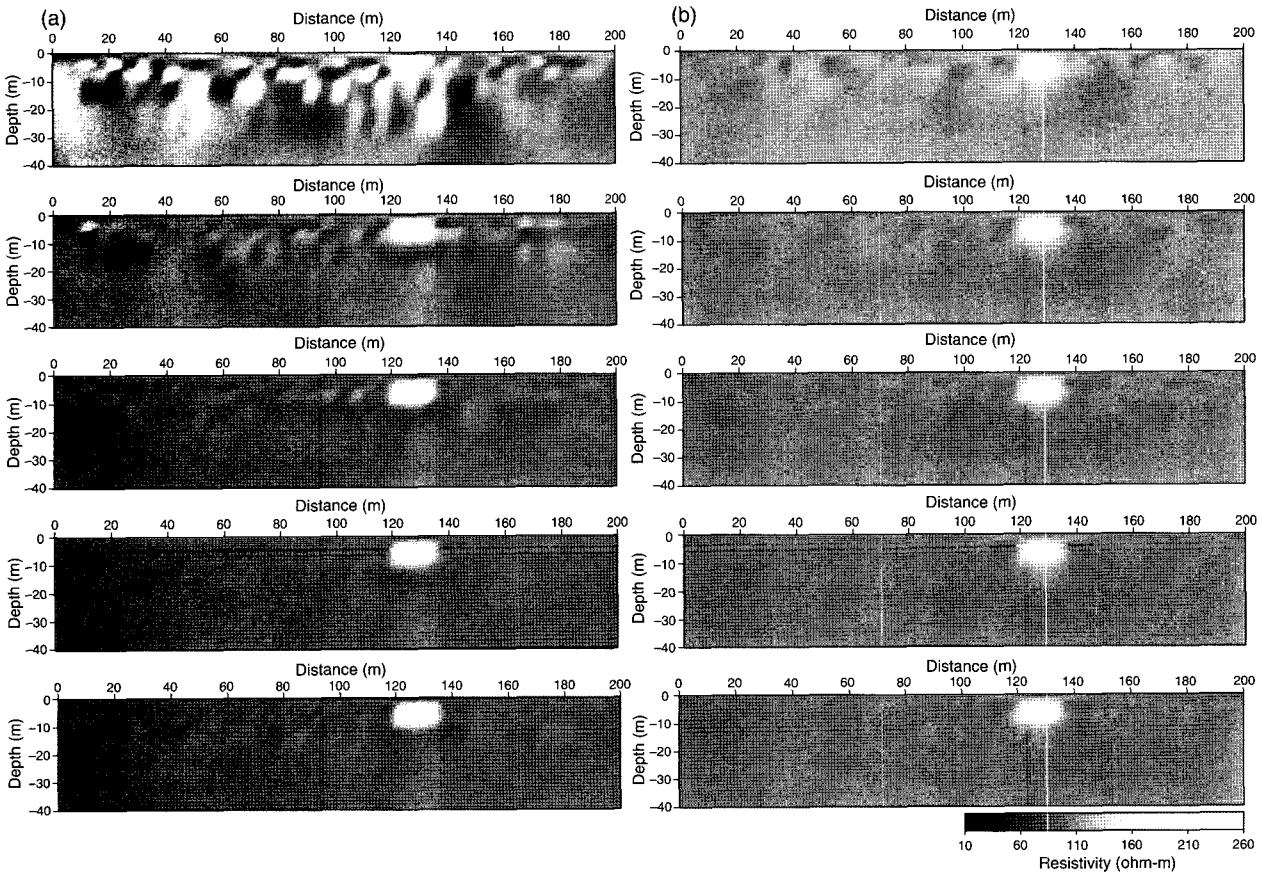

Fig. 2. Comparison of resistivity sections from multi-frequency IP inversion. (a) The inverted resistivity sections obtained by the independent inversion of datasets having different noise levels. (b) The results where all the IP datasets were simultaneously inverted using the cross regularisation scheme. The noise levels are 30, 10, 5, 2, and 2% respectively, from the top section down. Artefacts shown in the highest noise case (at the top) were effectively reduced by the cross regularisation scheme. The corresponding phase sections are shown in Figure 3.

representation of all individual single frequency IP inversions described in equation (6). Off-diagonal terms come from the cross regularisation, and the choice of another Lagrange multiplier β is an important issue in this inversion algorithm. We selected 0.5 as a value for β after a trial of various different values. This value of β is half of the diagonal element of smoothness constraint operator $\mathbf{W}_m$, which has the value of one. The sum of individual misfits for the single-frequency inversion is used as a misfit function in the multi-frequency inversion. In our trial inversion for the synthetic dataset, five iterations were enough for convergence of the inversion. All the results provided in this paper were found after five iterations.

Estimation of SIP parameters

SIP parameters are extracted from the inverted complex resistivities, estimated as a function of frequency, by fitting them to a pre-selected dispersion model. We use a modified Levenberg–Marquardt algorithm. The spectral parameters are estimated by minimising the squared differences between the inverted and estimated complex resistivities for the entire frequency range. Although any kind of dispersion model can be selected in this algorithm, we select the simple and well known Cole–Cole model to test the estimation algorithm.

In the Cole–Cole model, the complex resistivity at the frequency ω_k is given by

$$\rho(\omega_k) = \rho_{oj}\left(1 - \eta_j\left(1 - \frac{1}{1 + (i\omega_k\tau_j)^{c_j}}\right)\right) \qquad (10)$$

where ρ_{oj} is the DC resistivity, η_j is the chargeability, τ_j the time constant and c_j is the relaxation constant in the discretised subsurface. The effects of changes in different Cole–Cole parameters on the measured value are quite different. The changes in the time and relaxation constant have much smaller effects on the measured potential values compared to the resistivity and chargeability. This makes it possible to estimate the resistivity and chargeability more accurately compared to the time and relaxation constants (Loke et al., 2006). They introduce a multi-step inversion strategy to overcome the difficulty in estimating the time and relaxation constants in their approach. In this study, however we did not apply such multi-step strategy because our most important concern is to have more flexibility in the selection of a dispersion model.

Results and discussions

Figure 1 shows the simple subsurface model to test the new multi-frequency SIP inversion algorithm. Two anomalous blocks with different material properties are embedded in a homogenous and slightly polarizable background. One block exhibits a phase anomaly and the other shows a resistivity anomaly only. In this model, anomalous blocks are more polarizable or resistive than background. Spectral characteristics of the subsurface are not considered in this model because the main concern of this example is to test the new multi-frequency inversion method. Instead of using multi-frequency databased on the spectral characteristics or dispersion model, we prepared five synthetic IP datasets contaminated with different noise levels. The noise

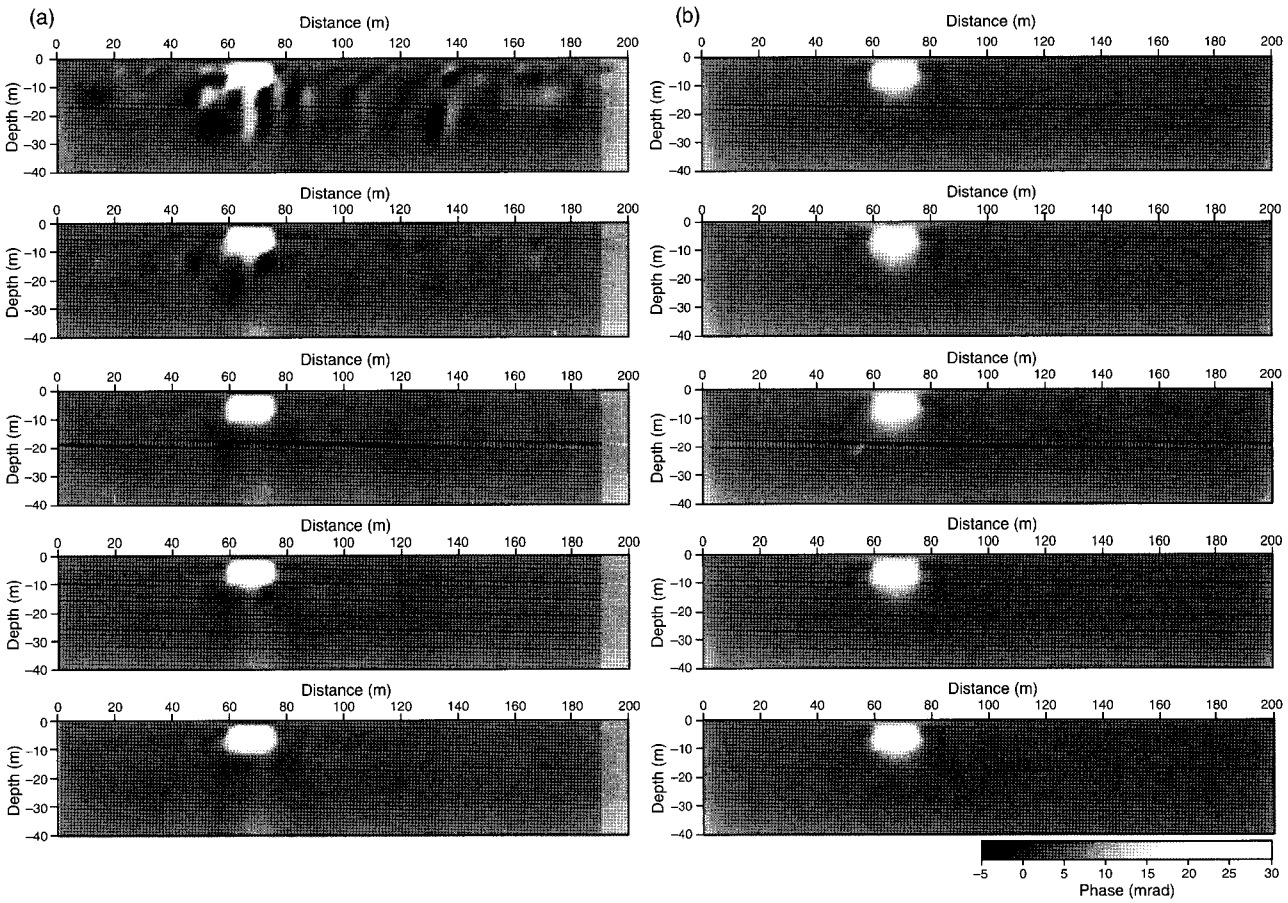

Fig. 3. Comparison of phase sections from the multi-frequency IP inversion. (a) The inverted phase sections obtained by the independent inversion of datasets having different noise levels. (b) The results where all the IP datasets were simultaneously inverted using the cross regularisation scheme. The noise levels are 30, 10, 5, 2, and 2% respectively, from the top section down. Artefacts shown in the highest noise case (at the top) were effectively reduced by the cross regularisation scheme. Corresponding resistivity sections are shown in Figure 2.

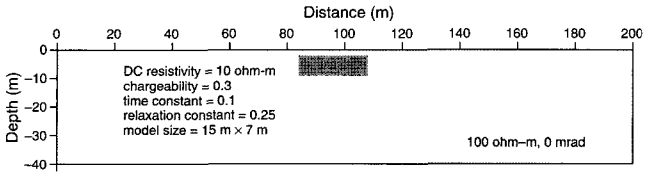

Fig. 4. Simple subsurface model to test the spectral parameter estimation algorithm. A conductive and polarizable anomaly is embedded in a non-polarizable homogeneous background. The Cole–Cole parameters are: DC resistivity is 10 Ω m, chargeability is 0.3, while time constant and relaxation constant are 0.1 s and 0.25 respectively. The size of block is 15 m × 7 m, and the number of frequencies is nine, evenly distributed in the frequency range of 0.01 to 100 Hz. A dipole–dipole array is used with dipole spacing of 5 m.

levels of each dataset are 30, 10, 5, 2, and 2% respectively. A dipole–dipole array layout, with dipole spacing of 5 m was used in this study. These datasets were inverted simultaneously by the new multi-frequency inversion algorithm to examine its performance.

Figure 2 shows the resistivity sections from the inversion of the five synthetic datasets with different noise levels. Panels shown on the left are the results without cross regularisation, while the right side shows the results when cross regularisation is used in the inversion. As expected from the noise level, we can see many artefacts in the inverted section for the data contaminated by 30% noise. These artefacts are also shown in the inverted sections for lower noise contents of 10%, 5% (second and third data from the top) although the magnitude is reduced. When cross regularisation is applied, on the other hand, artefacts are greatly suppressed in all five inverted images although some artefacts still remain in the image with the highest noise content. In this example, inversion with cross regularisation provides smoother results than independent inversion. However, the boundaries of anomalous blocks are smoothed and resistivity estimates are lower than for individually inverted models because of higher regularisation in the inversion.

Figure 3 shows the inverted phase sections corresponding to Figure 2. We can see very similar behaviour to that observed in

Table 1. Modelling parameters used for the model shown in Figure 4.

Dataset no.	1	2	3	4	5	6	7	8	9
Frequency [Hz]	0.01	0.032	0.1	0.32	1.0	3.2	10	32	100
Noise level [%]	5	20	5	2	30	5	10	2	5
Resistivity [Ω m]	9.37	9.20	9.02	8.81	8.60	8.37	8.15	7.95	7.77
Phase [mrad]	−21.58	−25.57	−29.29	−32.49	−34.60	−35.38	−34.67	−32.56	−29.45

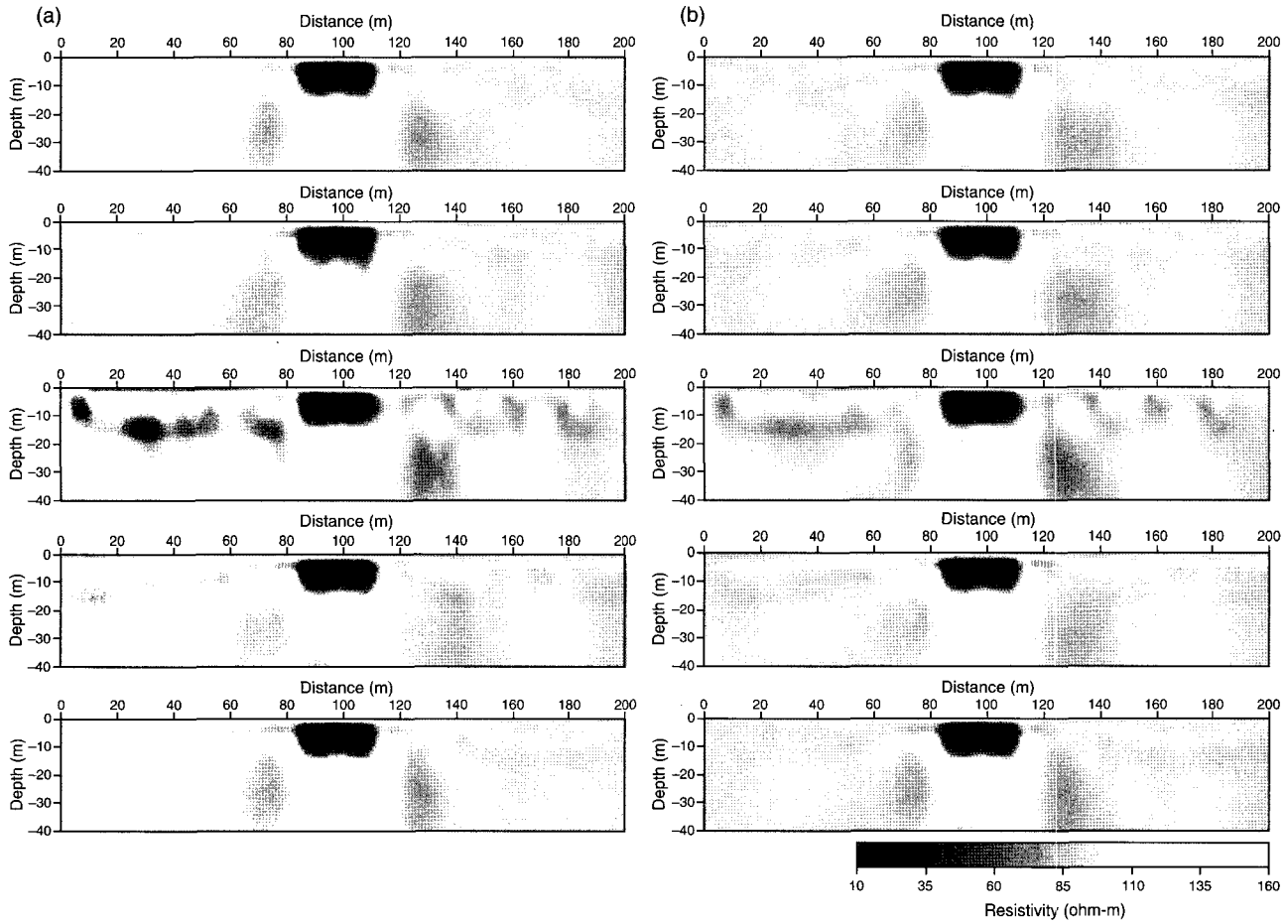

Fig. 5. Inverted resistivity sections obtained by the multi-frequency IP inversion of synthetic IP data for the model shown in Figure 4. Each figure shows the resistivity images for the frequencies of 0.01, 0.1, 1, 10, and 100 Hz from the top, respectively. Corresponding phase sections are shown in Figure 6. Left figures (a) show the results inverted without cross regularisation and right figures (b) shows the results with cross regularisation.

the resistivity sections. Artefacts can be seen in the individually inverted sections, while they are effectively removed in the inverted phase sections when cross regularisation is used in the inversion. The boundaries of anomalous blocks are more smoothed and phase value estimates are lower than for individually inverted models as in Figure 2. Although there is some loss in spatial resolution compared to the individually inverted results, inversion artefacts are greatly reduced by adopting cross regularisation in this example. This fact suggests that our regularisation scheme is very effective in suppressing the effect of noise, even when some erroneous data is included in the series of multi-frequency IP data. Our new regularisation emphasises the similar or common structure in the inverted section whether it is a real structure or not. Thus, it would be highly possible to emphasise noisy structure if coherent noise were present in the multi-frequency IP data. Care should therefore be taken in applying this cross regularisation to real field data.

Figure 4 shows the synthetic subsurface model used to test the SIP parameter estimation algorithm developed in this study. The model has only a 15 × 7 m anomalous block, located from 2.6 to 9.6 m depth in a non-polarizable homogeneous half-space medium. The Cole–Cole parameters of anomalous body were: the DC resistivity is 10 Ω m, the chargeability is 0.3, the time constant is 0.1 s, and the relaxation constant is 0.25, respectively. The number of frequencies was set to nine, and chosen in the frequency range from 0.01 to 100 Hz to give a linear distribution in logarithm scale. For the nine frequencies, synthetic IP data were modelled with the complex resistivity values calculated from the given spectral parameters. These nine IP datasets constitute the multi-frequency IP data, and our multi-frequency IP inversion algorithm was applied to obtain subsurface complex resistivity distributions. The multi-frequency IP data were contaminated with the different level of random noise in the range from 2 to 30%. Modelling parameters, such as noise level, frequency, resistivity, and phase of the anomalous body, are summarised in the Table 1. A dipole–dipole electrode array with dipole spacing 5 m was also used in this synthetic test.

Figures 5 and 6 show the inverted complex resistivities in terms of the amplitude (resistivity) and phase sections for the synthetic multi-frequency IP dataset, respectively. Individually inverted complex resistivities are also shown in the left side of each figure for the purpose of comparison. Images for five frequencies of 0.01, 0.1, 1, 10, and 100 Hz are shown in these figures. Since the variation of resistivity with frequency is very small (7.768 to 9.366 Ω m), noticeable differences are not seen in the each inverted resistivity sections in Figure 5. Due to the different noise levels, different artefact behaviours are also shown in the resistivity sections inverted individually. The anomalous body, however, is clearly imaged in all of these sections. Comparing the two results inverted with and without cross regularisation, the amplitude of artefacts is effectively reduced with cross regularisation, but artefacts caused by noise are still slightly evident in the data with greatest noise, the 1 Hz dataset. Due to cross regularisation in the inversion, all five sections show very similar resistivity structure. In the inverted phase sections (Figure 6), the anomalous body was also clearly

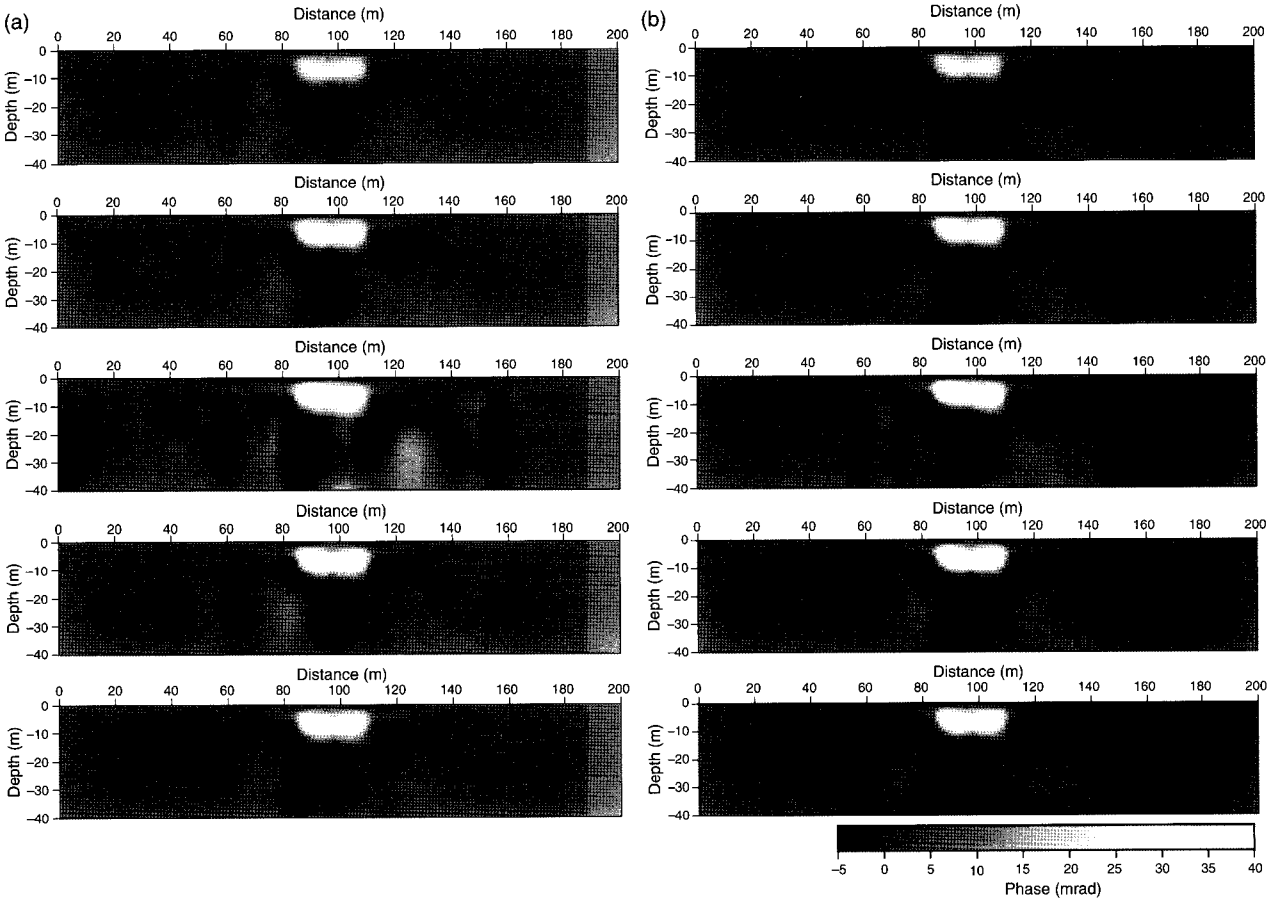

Fig. 6. Inverted phase sections obtained by the multi-frequency IP inversion of synthetic IP data for the model shown in Figure 4. Each figure shows the phase images for the frequencies of 0.01, 0.1, 1, 10, and 100 Hz from the top, respectively. Corresponding resistivity sections are shown in Figure 5. (a) The results inverted without cross regularisation and right figures (b) The results with cross regularisation. Note that the phase polarity is reversed in this plot for display.

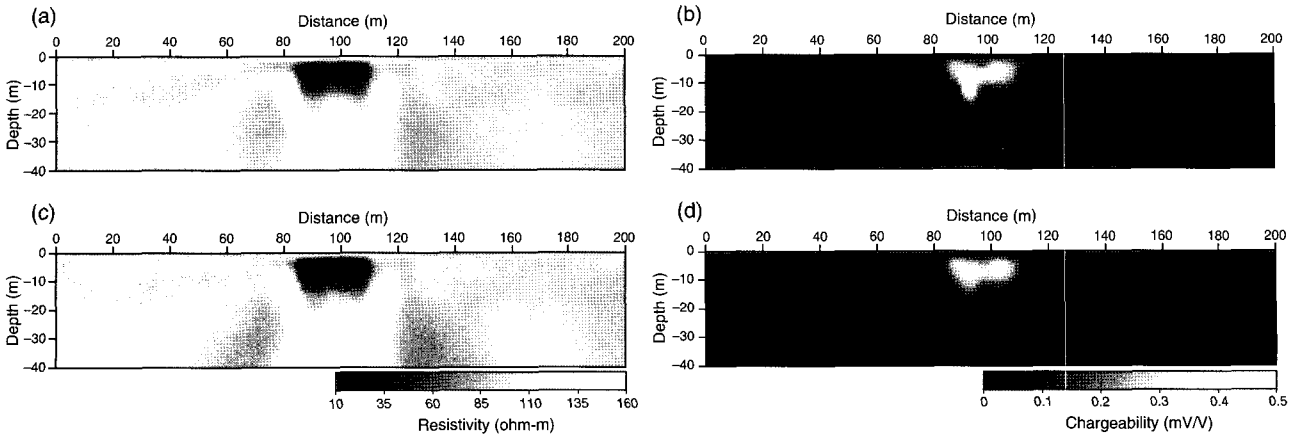

Fig. 7. Images of SIP parameters obtained by the inversion of the complex resistivities shown in Figures 5 and 6 (amplitude and phase of complex resistivity). (a) The DC resistivity and (b) chargeability obtained from the individually inverted complex resistivities. (c) The DC resistivity and the (d) chargeability from the complex resistivities inverted with cross regularisation.

imaged. Comparing the phase section inverted with and without cross regularisation, the effect of artefacts is also reduced by cross regularisation, but slight artefacts remain in the section with highest noise content. Compared to the resistivity section in Figure 5, the phase value of anomalous body shows somewhat larger variation with frequency. The phase value ranges from 21.578 to 35.270 mrad in the anomalous region. Due to this larger variation in phase, the differences are easier to observe than in the case of resistivity images. Although there are some variations in the phase values with frequency, all the phase sections show very similar images owing to cross regularisation, as in the case of resistivity section in Figure 5.

As the second step in obtaining spectral parameters, we applied the spectral parameter estimation algorithm to the inverted set of nine complex resistivity sections shown in Figures 5 and 6 (amplitude and phase of complex resistivity are shown in these figures). Figure 7 shows the spatial distribution of estimated DC resistivity and chargeability calculated from the inverted complex resistivities. For the purpose of comparison, the spatial distribution calculated from the individually inverted complex resistivities are also shown in the figure. Before applying the estimation algorithm to the inverted complex resistivities of each inversion block, we need to decide whether the inversion block possesses spectral properties or not. The inverted complex resistivity can have small phase values even though the spectral property is not present in the true model. This phase noise hinders the correct estimation of spectral parameters, especially the time and relaxation constants. To obtain reasonable estimates of spectral parameters, the maximum allowable absolute phase value was set to 3 mrad and only blocks having average phase greater than this threshold were chosen for the estimation of spectral parameters. Since our estimation algorithm used in this study is not optimised for the calculation of the relaxation and time constant, only the DC resistivity and chargeability images are shown. In Figure 7, the anomalous body is clearly imaged in both the DC resistivity and chargeability sections, and their values are very close to the exact values in Figure 4. Comparing the results which are inverted with and without cross regularisation, the distribution of DC resistivity shows very similar structures. If a block does not have spectral properties, we use the average value of inverted resistivities as its DC resistivity, which may cause the two distributions of DC resistivity to look similar. The selection of block which does has spectral properties makes the distribution of chargeability looks uniform because only the blocks with spectral properties are used for the inversion of spectral parameters. It may also be another factor, that the fluctuations of complex resistivity are smoothed during the inversion of spectral parameters. However, the chargeability distribution obtained from the inverted results with cross regularisation is smoother than those from the individually inverted results. Although the images of relaxation and time constant are not smooth enough to display as a section, the anomalous block also shows a very good match with the exact spectral parameters.

To evaluate the accuracy of the spectral estimation results, the values of the Cole–Cole parameters of the inverse block in the anomalous body obtained in the estimation are summarised in Table 2. All the parameters are slightly overestimated except the time constant but are very close to the original values, which suggest that our two-step inversion algorithm to obtain SIP parameters is a very accurate and reasonable approach. Comparing the results estimated from the complex resistivities inverted with and without cross regularisation, the spectral parameters obtained from the data inverted with cross regularisation are closer than those from the data inverted individually.

Figure 8 shows the input complex resistivity and that calculated from the estimated spectral parameters in Table 2. The complex resistivities were compared by plotting the resistivity and phase in the figure, and the estimated resistivity and phase shows a very good match with the input complex resistivity. The resistivities and phases inverted with cross regularisation have smaller fluctuations than the individually inverted results. As we notice in the figure, the resistivities are overestimated compared with the original values, but the trend with frequency is very similar to the original value. In the phase curve with frequency (Figure 8b), the shape of the curve is more complex than for resistivity. The individually inverted phase value shows larger fluctuations than that inverted with cross regularisation. Although the phase curve does not exactly match the original, its variation shows very similar behaviour. Minima of curvature obtained from the inverted complex resistivities with cross regularisation coincide with the input values, but in

Table 2. Comparison of estimated and exact spectral parameters of the centred anomalous block.

	Estimated value (individually inverted)	Estimated value (cross regularised)	Original (exact) value
DC resistivity	11.921	12.051	10.00
Chargeability	0.34115	0.30754	0.30
Time constant	0.08200	0.08029	0.10
Relaxation constant	0.22619	0.26223	0.25

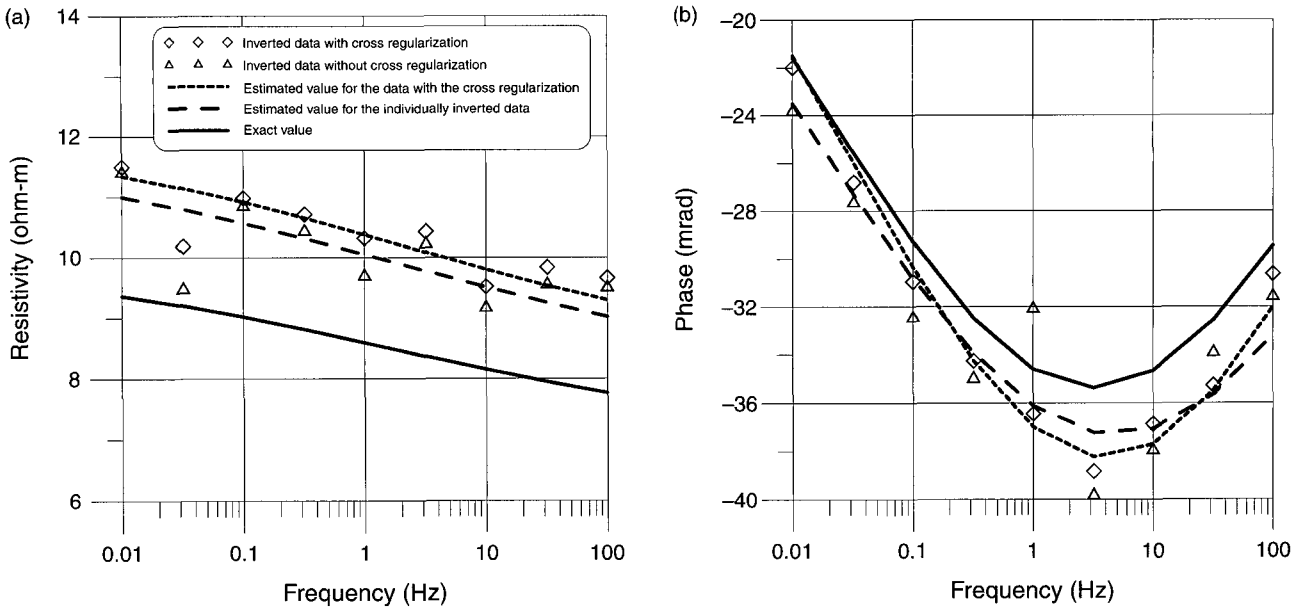

Fig. 8. Comparison of input complex resistivity and the complex resistivity calculated for the estimated spectral parameters in Table 2. (a) The amplitude of complex resistivity. (b) The phase.

the individually inverted case the minima are moved to higher frequencies. We also notice that the variation of resistivity and phase is quite small. In the frequency range used in this model, the resistivity shows a maximum variation of 2 Ω m, while the phase varies by 14 mrad. For the accurate estimation of SIP parameters, we should have very accurate complex resistivities for each frequency. Therefore, accurate IP data acquisition followed by multi-frequency inversion with fewer artefacts is crucial to the good estimation of spectral parameters.

Conclusions

In this study, we developed a multi-frequency IP inversion algorithm adopting the cross regularisation method. Cross regularisation was applied to minimise the difference between model update vectors at adjacent frequencies. By numerical experiments, we could show that our new inversion method could effectively reduce the inversion artefacts and provide more accurate and reasonable results than those obtained without cross regularisation. This cross regularisation in the multi-frequency inversion algorithm makes up for weak points in the indirect approach for the estimation of spectral parameters in this study.

We have also developed an estimation algorithm for spectral parameters from inverted complex resistivity, based on the modified Levenberg–Marquardt method. The Cole–Cole model was used as a dispersion model in this estimation algorithm. In this method, we first decide whether each inversion block has spectral characteristics or not to avoid erroneous calculation. Inversion blocks having average absolute phase values larger than 3 mrad are selected for the estimation of Cole–Cole parameters. Since our estimation is done by an indirect approach, the distribution of spectral parameters obtained, especially of the time and relaxation constants, is not smooth enough to be interpreted directly. The estimated values of spectral parameters for the anomalous block do show a good match with the true model. Even though our estimation algorithm is not optimised and does not consider the low sensitivity of time and relaxation constants in the Cole–Cole dispersion model, very reasonable SIP parameters, close to original values, could be obtained, which validates our two-step approach to obtain SIP parameters. Therefore, we can say that the two-step multi-frequency IP inversion technique developed in this study can be used to obtain the spectral parameters, and that the SIP method will provide valuable information on the subsurface physical properties other than resistivity, for use in the field of engineering and environmental problems.

Acknowledgments

This research was supported by the Basic Research Project of the Korea Institute of Geosciences and Mineral Resources (KIGAM), funded by the Ministry of Science and Technology of Korea.

References

Börner, F. D., Gruhne, M., and Schön, J. H., 1993, Contamination indications derived from electrical properties in the low frequency range: *Geophysical Prospecting* **41**, 83–93. doi: 10.1111/j.1365-2478.1993.tb00566.x

deGroot-Hedlin, C., and Constable, S. C., 1990, Occam's inversion to generate smooth, two-dimensional models from magnetotelluric data: *Geophysics* **55**, 1613–1624. doi: 10.1190/1.1442813

Fink, J. B., McAlister, E. O., Sternberg, B. K., Wieduwilt, W. G., and Ward, S. H. (eds), 1990, *Induced Polarization*, Society of Exploration Geophysics.

Kemna, A., Binley, A., Ramirez, A. L., and Daily, W. D., 2000, Complex resistivity tomography for environmental applications: *Chemical Engineering Journal* **77**, 11–18. doi: 10.1016/S1385-8947(99)00135-7

Kemna, A., Binley, A., and Slater, L., 2004, Crosshole IP imaging for engineering and environmental applications: *Geophysics* **69**, 97–105. doi: 10.1190/1.1649379

Loke, M. H., Chambers, J. E., and Ogilvy, R. D., 2006, Inversion of 2D Spectral induced polarization imaging data: *Geophysical Prospecting* **54**, 287–301.doi: 10.1111/j.1365-2478.2006.00537.x

Olhoeft, G. R., 1985, Low-frequency electrical properties: *Geophysics* **50**, 2492–2503. doi: 10.1190/1.1441880

Pelton, W. H., Ward, S. H., Hallof, P. G., Sill, W. R., and Nelson, P. H., 1978, Mineral discrimination and removal of inductive coupling with multifrequency IP: *Geophysics* **43**, 588–609. doi: 10.1190/1.1440839

Routh, P. S., Oldenburg, D. W., and Li, Y., 1998, Regularized inversion of spectral IP parameters from complex resistivity data: *68th Annual International Meeting, Society of Exploration Geophysicists, Expanded Abstracts*, 810–813.

Vanhala, H., Soininen, H., and Kukkonen, I., 1992, Detecting organic chemical contaminants by spectral-induced polarization method in glacial till environment: *Geophysics* **57**, 1014–1017. doi: 10.1190/1.1443312

Weller, A., and Börner, F. D., 1996, Measurement of spectral induced polarization for environmental purposes: *Environmental Geology* **27**, 329–334. doi: 10.1007/s002540050066

Yang, J. S., and Kim, H. J., 2004, Estimation of Cole–Cole parameters from multi-frequency IP data: *Journal of the Korean Society for Geosystem Engineering* **41**, 228–234.

Yi, M. J., Kim, J. H., and Chung, S. H., 2003, Enhancing the resolving power of least-squares, inversion with active constraint balancing: *Geophysics* **68**, 931–941. doi: 10.1190/1.1581045

Yuval, and Oldenburg, D. W., 1997, Computation of Cole–Cole parameters from IP data: *Geophysics* **62**, 436–448. doi: 10.1190/1.1444154

Manuscript received 14 December 2006; accepted 31 January 2007.

다중 주파수 IP 자료를 이용한 SIP 변수 추정

손정술, 김정호, 이명종

요 약: 광대역 유도 분극 (spectral induced polarization, SIP) 탐사는 일정 주파수 영역에서 임피던스 자료를 측정하고, 이 자료로부터 광대역 주파수 특성을 추정하기 위한 주파수 분석으로 이루어진다. 지하매질에 대한 광대역 주파수 특성을 정확하고 정량적으로 추정하기 위해서는 기존의 방법보다 정교하고 안정적인 역산 알고리듬이 필요하다. 이를 위해 이 연구에서는 SIP 변수의 공간적인 분포를 계산하기 위하여 두 단계로 이루어진 역산 알고리듬을 개발하였다. 첫 번째 단계에서 각각의 주파수 자료에 대한 복소 전기비저항들 사이에 제한조건을 가하여 모든 SIP 탐사자료를 한꺼번에 역산한다. 새로운 제약조건은 각각의 주파수 자료들로부터 역산된 복소 전기비저항들이 모두 유사한 특성을 보일 것이라는 가정을 통해 역산 과정에서의 잡음 특성을 향상시킬 수 있는 특징을 가진다. 수치 실험을 통하여 이 연구에서 채택한 상호 제한 조건은 역산 과정상의 인위적인 잡음을 성공적으로 제거하고 있음을 확인하였다. 두 번째 단계로서 이전 단계에서 얻어진 각각의 주파수에 대한 복소 전기비저항 자료로부터 SIP 변수의 공간적인 분포를 계산하기 위하여, Cole-Cole 모델을 이용하여 SIP 변수들을 역산을 통해 계산하게 된다. 수치 실험을 통하여 역산된 SIP 변수의 영상이 실제 모델과 잘 일치하고 있음을 확인하였다. 개발된 SIP 해석기법은 일반적인 전기비저항 탐사보다 유용한 지하 영상을 제공할 수 있을 것으로 기대된다.

주요어 : 광대역 유도분극 탐사, 복소 전기비저항, 역상, 상호 제한조건, Cole-Cole 모델, SIP 변수

マルチ周波数 IP データからのスペクトル IP パラメータ評価

孫 正述（ソン・ジョンスル），金 槙浩（キム・ジョンホ），李 明鍾（イ・ミョンチョン）

要 旨: IP 法は，多孔質地盤の構造や水理特性そして地下流体についての貴重な情報を我々に提供することができる方法である。IP 法の適用により，複素比抵抗解析を経て，電気伝導度から表面伝導の効果を分離することができ，より岩相に即した特性評価が可能となる。さらに，地盤のスペクトル応答を複素比抵抗のいくつかの組合せから推定することができる。一般に，スペクトル IP 法の測定は印可する電流の周波数に対して実施される。そして，これらの周波数における測定データを使用してスペクトル解析が行われる。本研究では，分散モデルの選択における柔軟性を最大限にするために，逆解析により推定された個々の複素比抵抗値からスペクトルパラメータを評価するという間接的なアプローチを選択した。この間接的アプローチ適用に際して，精度の高いスペクトルパラメータの評価のために，より安定した逆解析アルゴリズムが要求される。我々は，それぞれの周波数に対するデータから推定した比抵抗断面図を相互に正則化し，全ての周波数におけるデータを同時に使用して，スペクトルパラメータを推定する新しい逆解析手法を提案した。この手法では，個々の周波数におけるデータから推定した複素比抵抗値を，他の周波数に対して推定した複素比抵抗値と同じになるように正則化を与えている。新しい正則化手法により，データセット全体に含まれるノイズの影響は改良される。数値実験において，この逆解析アルゴリズムはノイズに起因するランダムな構造を効果的に減少できることが確認された。スペクトルパラメータの推定に際しては，コール・コールモデルを採用し，逆解析により求められた複素比抵抗値からコール・コールモデルのパラメータを修正レーベンバーグ・マルカート法により推定した。我々はスペクトルパラメータの推定において，間接的なアプローチを選択したが，推定したパラメータは平滑な分布ではなく，真の値によく整合したものであった。

キーワード：マルチ周波数逆解析，複素比抵抗，スペクトル IP，コール・コールモデル

한국지질자원연구원 지반안전연구부
305-350, 대전 유성구 가정동 30

韓国地質資源研究院 地盤安全研究部